A new methodology for inferring surface ozone from mutltispectral satellite measurements

Nadia Colombi,[1*] Kazuyuki Miyazaki,[2*] Kevin W. Bowman,[2*] Jessica L. Neu,[2*] and Daniel J. Jacob[1*]

[1]Harvard University, Department of Earth and Planetary Sciences, Boston, MA, United States.

[2]Jet Propulsion Laboratory, California Institute of Technology, Pasadena, CA, United States.

E-mail: ncolombi@g.harvard.edu

Abstract.

Over the past two decades, satellite instruments have provided unprecedented information on global air quality, and yet the remote sensing of surface ozone remains elusive. Here we propose a new method to infer spatial gradients in surface ozone by combining multispectral ozone retrievals using radiances from the Tropospheric Emission Spectrometer (TES) thermal infrared (TIR) instrument and the Ozone Monitoring Instrument (OMI) ultratraviolet/visible (UV/VIS) instrument with a chemical reanalysis. We find that our inferred surface ozone in summertime China and the United States has regional biases of less than 4 ppb and a high spatial correlation when validated against independent surface measurements. Over the broader Asia region, our analysis results in a spatial pattern of summertime surface ozone that can largely be explained by a combination of the Asian monsoon circulation and NO_x emissions. Our results show the potential of combining satellite measurements and chemical reanalyses to provide critical air quality information in regions of limited surface networks, thereby augmenting the global air quality observing system.

1. Introduction

Tropospheric ozone is a greenhouse gas and pollutant that is detrimental to human health and ecosystem productivity. While particulate matter accounts for much of the health risk from air pollution, ozone exposure was responsible for 427,000 premature deaths from chronic obstructive pulmonary disease (COPD) in 2017, most of which occurred in South and East Asia [1]. Ozone also damages plant metabolic function and is responsible for $11-18 billion USD in crop losses each year [2]. Nevertheless, the current ground-based measurement network is not sufficient to monitor ozone changes, especially in developing countries [3].

Over the last two decades, satellite-based measurements of the ozone column and its vertical distribution have played an increasingly important role in global tropospheric ozone monitoring [4]. These measurements exploit ozone molecular absorption in the ultraviolet (UV, Hartley and Huggins band), visible (VIS, Chappuis band), and the thermal infrared (TIR) [5]. UV/VIS instruments measure ozone by backscatter of solar radiation from the Earth's surface, with sensitivity to the lower troposphere limited by atmospheric scattering [6]. The Chappuis bands are less limited by molecular and aerosol scattering but they are very weak, resulting in low signal to noise. In addition to low surface sensitivity, UV backscatter instruments provide limited information on the vertical distribution of tropospheric ozone [7] [8], [9]. TIR instruments provide more vertical information by measuring ozone via thermal emission from the atmosphere, but sensitivity to the lower troposphere is limited by clouds and low temperature contrast with the surface [6].

The global distribution of tropospheric ozone has been retrieved from the Global Ozone Monitoring Experiment (GOME) and Ozone Monitoring Instrument (OMI) [8–10]. OMI and GOME retrievals typically have 0.5-1.5 Degrees of Freedom for Signal (DOFS-a measure of the independent pieces of information in the retrieval [11]) for the troposphere, which limits the measurements to total or tropospheric columns [7]. The Tropospheric Emission Spectrometer (TES) typically provides 1.6 DOFS in the troposphere and thus provides information about the tropospheric profile, generally limited to the free troposphere above 3 km altitude [7, 12–14]. These limitations extend to more recent TIR sounders such as the Infrared Atmospheric Sounding Interferometer (IASI) [15] and the Cross-track Infrared Sounder (CrIS) [16].

Over the last decade, the idea of combining TIR and UV radiances as a way to enhance sensitivity to ozone in the lower troposphere has been explored [7, 12, 14, 17, 18]. [14] were able to observe the spatial distribution of ozone plumes in the lowermost troposphere using combined TIR radiances from IASI and UV radiances from GOME-2. The joint TES/OMI retrieval, which combines the radiances measured by the two instruments on the Aura satellite provides 2 DOFS in the troposphere with improved sensitivity to the lowest 3 km column with DOFS of up to 0.4 in that altitude range [19]. While it has been established that TES/OMI provides enhanced sensitivity to lower tropospheric column ozone compared to either instrument alone, the relationship of lower tropospheric column to surface ozone has not been fully explored.

To that end, we propose a new method to evaluate spatial gradients in surface ozone using the TES/OMI multispectral retrievals, in conjunction with information provided by a well-validated chemical reanalysis product [20] as a transfer function. The chemical reanalysis provides information about the spatio-temporal relationship between the lower tropospheric ozone column and surface ozone. The surface ozone inferences are then evaluated against independent ground truth observations from the relatively dense surface measurement networks. While the proof-of-concept of this methodology

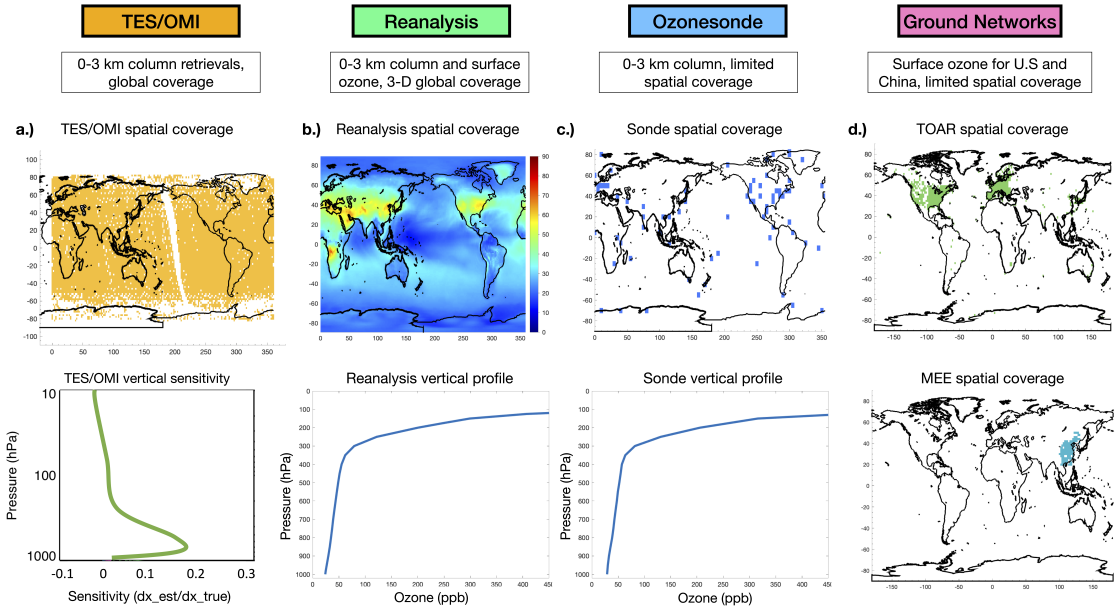

Figure 1. Overview of the characteristics of data used in this study. The images in the top row illustrate the spatial capabilities of each of these data, whereas the bottom row highlights their ability to detect the vertical ozone profile for (a)-(c). For (d), each of the rows in the ground networks column highlights the spatial extent of the two surface monitoring networks used in this study. (a) The TES/OMI satellite retrievals provide global coverage of ozone profiles (top row) with enhanced sensitivity to approximately the lowest 3 km (bottom row). The sampling density shown here represents 3 months of data (June, July, August) from each year for 2005-2009. (b) The chemical reanalysis provides gridded complete global data of ozone (top row) at each level throughout the troposphere. (c) The ozonesonde measurements provide vertical profiles of ozone but with limited spatial and temporal coverage. (d) The in-situ surface ozone stations used in this study include the TOAR (top row) and MEE (bottom row) networks.

is demonstrated with TES/OMI retrievals, the proposed approach itself can be applied more generally to other satellite datasets with sensitivity to the lower troposphere, e.g., AIRS+OMI [16], which provides increased coverage by 2 orders of magnitude compared to TES/OMI.

2. Data

2.1. TES/OMI ozone retrievals

We use the joint ozone retrieval product from TES and OMI [19] (Fig. 1a), both of which are on the Aura spacecraft. The NASA Aura platform was launched in 2004 in a near-polar, sun-synchronous, 705 km altitude orbit whose ascending node has a 13:38 equator crossing time. TES is a Fourier transform spectrometer that measures radiances in the TIR (650-3050 cm^{-1}) with an apodized spectral resolution of about 0.1 cm^{-1} in

the nadir. TES measurements provide a single nadir profile, with a footprint size of 5.3 km (across track) x 8.5 km (along the spacecraft ground track), every 182 km along track [21]. The revisit time is 16 days. TES global measurements ended in 2011 and were switched to targeted observation mode until decommissioning in 2018.

OMI is a nadir-viewing push broom ultraviolet-visible (UV-VIS) imaging spectrometer. OMI provides global measurements of backscattered radiances covering the 270-500 nm wavelength range, with the ground pixel size at nadir position of 13 km (along the ground track) × 24 km (across track). Unlike TES, OMI is a swath instrument that samples 2600 km across-track. However, only the OMI pixel closest to the TES footprint is used.

The TES and OMI retrieval algorithms are based upon optimal estimation, which executes a nonlinear optimization algorithm that minimizes the difference between observed and simulated radiances subject to prior knowledge of second-order statistics [22]. This framework leads to formal characterization of error statistics and observation operators (averaging kernels) needed for model evaluation and assimilation [23, 24].

The joint TES/OMI retrieval algorithm builds on the operational TES retrieval algorithm but integrates radiances from both instruments [12, 19]. While TES typically provides 1.6 DOFS and OMI provides less than 1 DOFS for the troposphere, the joint TES/OMI (Fig. 1a) provides 2 DOFS for the troposphere with approximately 0.4 DOFS for near surface ozone in average (surface to 700 hPa, [19], Fig. S1). We excluded TES/OMI data with the 0-3km column DOFS of less than 0.2 and those with a poor quality control flag. Approximately 7,000 TES/OMI profiles were available after the filtering for the United States and China for the 2005-2009 summertime (June-August) period.

2.2. Surface ozone observations

The Tropospheric Ozone Assessment Report (TOAR) database [25] (Fig. 1d top row) provides the largest collection of global in-situ surface ozone data available; it combines nearly 10,000 measurement sites located in Europe, North America, and Japan. We used gridded (2×2°) hourly TOAR data at 13:00 local time, corresponding to the Aura overpass (https://doi.org/10.1594/PANGAEA.876108) to evaluate the satellite-derived surface ozone over the United States for 2005-2009.

We also used China's Ministry of Ecology and Environment (MEE) surface network (http://datacenter.mep.gov.cn/index) (Fig. 1d bottom row) that consists of 450 measurement sites and provides hourly data from 2013 to 2017. We used the MEE data at 13:00 local time. The MEE network data is only available after 2013. To evaluate the satellite-derived surface ozone during 2005-2009, the MEE data was converted from observed values in 2013-2017 to estimated values during the 2005-2009 period based on the mean temporal changes at each grid point in the chemical reanalysis. The estimated country-averaged surface ozone for summer months (JJA) is lower in 2013-2017 (50.4

ppb) than in 2005-2009 (56.9 ppb). This conversion approach provides observationally-constrained information on the 2005-2009 surface ozone. Nevertheless, in the chemical reanalysis, direct aerosol emissions and VOC emissions were not constrained by any observations. Because surface ozone responds to various factors, including the NO_x-VOC chemical regime, the unconstrained emissions could lead to a biased change from the 2005-2009 to 2013-2017 periods, which needs to be further addressed in a future study.

The two regions, China and the United States, were chosen due to their ample amount of surface ozone data for validation and for the fact that they have substantial spatial gradients in ozone across the countries. We focus our analysis on summer months, when the TES/OMI retrievals have the highest DOFS due to the high surface temperature (TES) and high solar elevation (OMI).

2.3. Chemical reanalysis products

We use a tropospheric chemistry reanalysis, which was produced using the assimilation of multiple updated satellite measurements of ozone, CO, NO_2, HNO_3, and SO_2 from multiple satellite instruments [20]. The global gridded ozone data from the chemical reanalysis provides vertical profiles of ozone for any given grid point across the globe (Fig. 1b).

Comparisons against independent aircraft, satellite, and ozonesonde observations demonstrate the quality of the analysed O_3, NO_2, and CO concentrations on regional and global scales and for both seasonal and year-to-year variations from the lower troposphere to the lower stratosphere [20]. The chemical reanalysis products have already been employed in various air quality studies [26], [27], [28] [29], [30], [31], [32].

2.4. Ozonesonde observations

The ozonesonde network (Fig. 1c) exhibits limited spatial coverage, but with robust vertical profiling capabilities from the surface to the stratosphere with a vertical resolution of approximately 150 m and an accuracy of $\pm 5\%$ [33]. The ozonesonde stations are mostly located in the northern hemisphere over the continents, with sampling intervals of typically 1-2 weeks.

While the ozonesonde network doesn't cover a dense geographical region, these measurements provide unique information to evaluate the bias in the chemical reanalysis product at the 0-3 km level for the 2005-2009 period. For the United States, we used ozonesonde measurements from 23 stations across the continental United States. For China, ozonesonde data from Hong Kong are used.

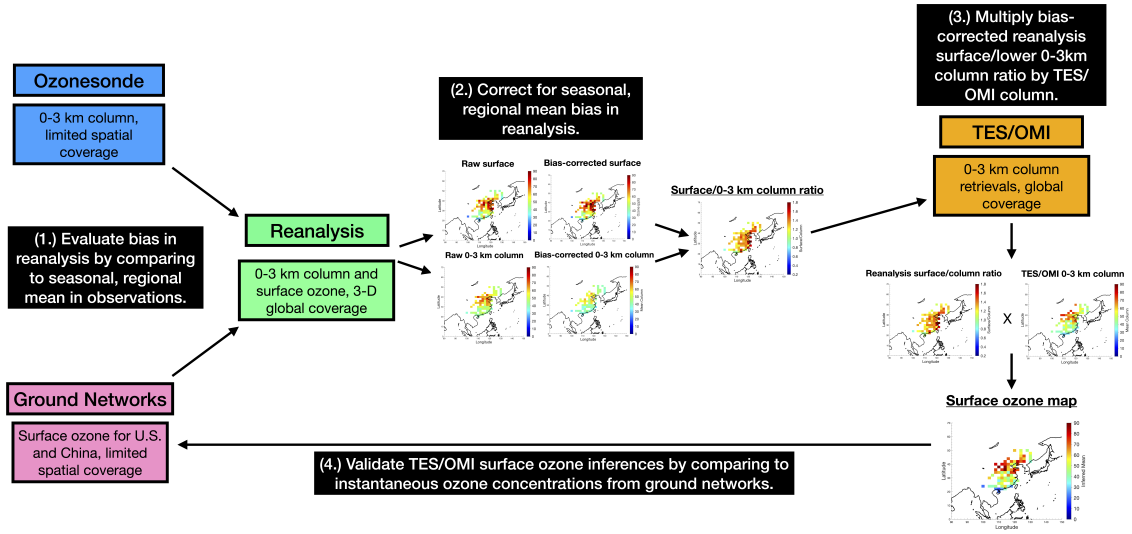

Figure 2. Schematic detailing how surface ozone inferences are made from TES/OMI lower tropospheric column measurements for China as an example. (1) The regional bias in seasonal mean ozone in the reanalysis is evaluated for both the surface and 0-3km column. (2) Bias corrections are made to the reanalysis based on the comparison results from (1). (3) The relationship between bias-corrected surface and 0-3 km column reanalysis is then used as a transfer function to infer surface ozone using the TES/OMI column retrievals. (4) These surface ozone inferences are validated against individual observations from the TOAR and MEE surface ozone networks.

3. Methodology

As illustrated in Fig. 2, the approach uses four different types of information in the following steps.

3.1. Reanalysis bias correction: 0-3 km column

The reanalysis provides the global spatial and vertical distributions of ozone. Nevertheless, its systematic bias could affect the accuracy of surface ozone estimation. To remove possible bias in the reanalysis 0-3 km column at regional and seasonal scales, we applied a bias correction using independent ozonesonde data for the western and eastern United States, and China, separately. The bias in the 0-3 km column ozone was evaluated by taking the seasonal, regional mean difference between the reanalysis and ozonesonde observations at ozonesonde sampling sites for each year during 2005-2009. Then, we take the spatial and multi-year average of the seasonal means of reanalysis and observation differences, so that we have one bias value for each region (step 1 in Fig. 2). The estimated bias is summarized in Section S1. We then subtracted the bias from all

0-3 km reanalysis data at all grid points within each region (step 2). The bias-corrected reanalysis uniquely provides spatial and temporal variability of the lower tropospheric column within each domain.

Because of the limited spatial coverage of the ozonesondes [34], the ability of the bias correction is limited, especially in China, where the only ozonesonde site is Hong Kong. Nevertheless, we note that the increase in surface ozone and decrease in 0-3 km ozone needed to match the observations in China (Figure 2) is consistent with excessive vertical mixing in the model boundary layer, which has been noted in other studies. A careful consideration of the measurement representativeness, considering atmospheric variability and sampling frequency, would benefit the bias correction [35].

3.2. Reanalysis bias correction: surface

The process for correcting bias in the reanalysis surface ozone concentrations is the same as that of the 0-3 km column, except we now use surface ozone observations from the TOAR and MEE networks to estimate seasonal and regional averaged surface ozone bias over the three regions (step 1). The use of the seasonal, regional mean in the bias correction ensures independence of the data used for calibration (step 2) versus validation (step 4). In the validation step, the TOAR and MEE networks provide unique information on the spatial and temporal variation of surface ozone against which to evaluate the ability of TES/OMI to capture these variations. For China, the MEE data converted to the 2005-2009 values are used. The estimated surface ozone bias is shown in Section S1.

3.3. Derive surface ozone from TES/OMI 0-3 km column

In step 3, the relationship between bias-corrected reanalysis 0-3 km column and reanalysis surface ozone is used as a transfer function to infer surface ozone from the TES/OMI 0-3 km column retrieval for each satellite pixel separately as follows:

$$r_{surf}(satellite) = r_{col}(satellite) \times \frac{r_{surf}(reanalysis)}{r_{col}(reanalysis)} \quad (1)$$

The ratio between bias-corrected reanalysis surface and 0-3 km column mean ozone concentration, $\frac{r_{surf}(reanalysis)}{r_{col}(reanalysis)}$, is multiplied by the TES/OMI 0-3 km column mean ozone concentration, $r_{col}(satellite)$, for overlapping grid points in time and space. The reanalysis surface versus 0-3 km column average ratio at each grid box is applied to TES/OMI 0-3 km column measurements to infer surface ozone concentrations. This approach allows us to determine whether TES/OMI can resolve spatial gradients in surface ozone.

3.4. Validation

The TES/OMI surface ozone inferences for the United States and China are directly compared to the TOAR and MEE observations. We focus our analysis on summer months, when TES/OMI has the highest DOFS. There are approximately 7000 TES/OMI profiles that match ground network observations during JJA of 2005-2009. We use standard major axis (SMA) regression, which assumes errors in both the x and y variables, to determine the spatial correlation between TES/OMI surface ozone inferences and network observations.

4. Results

4.1. Bias-Corrected Reanalysis Ozone Fields

The bias-corrected reanalysis shows a compact relationship between the surface and 0-3 km column over the TES/OMI sampling points (13:00 local time) for both the United States (Fig. 3a) and China (Fig. 3b), with a correlation coefficient of 0.83–0.86 and slope of the linear regression of 1.62 for China and 1.95 for the United States. The uncorrected reanalysis has similarly high correlation coefficients of 0.81 and 0.86, but shallower slopes of 1.3 and 1.7 for China and the United States, respectively. The steeper slopes after the bias correction likely reflect the underestimation of surface ozone in the western United States and overestimation of 0-3 km column ozone in China, respectively, in the reanalysis (Sections 3.1 and 3.2). The fact that the slopes are greater than 1 suggests a larger variability in surface ozone than in the LT column, with a positive vertical gradient under low surface ozone conditions and a negative vertical gradient when surface ozone is high. Taken together, these results indicate that it is very difficult to evaluate surface ozone directly from the 0-3 km column. The novel use of the reanalysis presented here represents an exciting new approach that accounts for the differences in vertical ozone gradients under different surface conditions.

4.2. Inferred Surface Ozone from TES/OMI Column (0-3 km)

4.2.1. The United States The satellite-derived surface ozone is evaluated against the surface measurements from the TOAR network for the United States (Fig. 4) and MEE network for China (Fig. 6) for each grid point for each day separately. The regional, summertime 2005-2009 mean for the western United States (30-50N, 100-125W) was 49.9 ppb for the TES/OMI 0-3 km averages (Fig. 4a) 51.6 ppb (95% confidence interval [49.5 53.7], based on error in reanalysis bias) for the TES/OMI surface inference (Fig. 4b) and 51.1 ppb for the TOAR network (Fig. 4c), whereas those for the eastern United States (25-50N, 65-100W) were 51.3 ppb, 42.7 ppb (95 % confidence interval [41.0 44.5], based on error in reanalysis bias) and 46.1 ppb, respectively. The low bias in the inferred

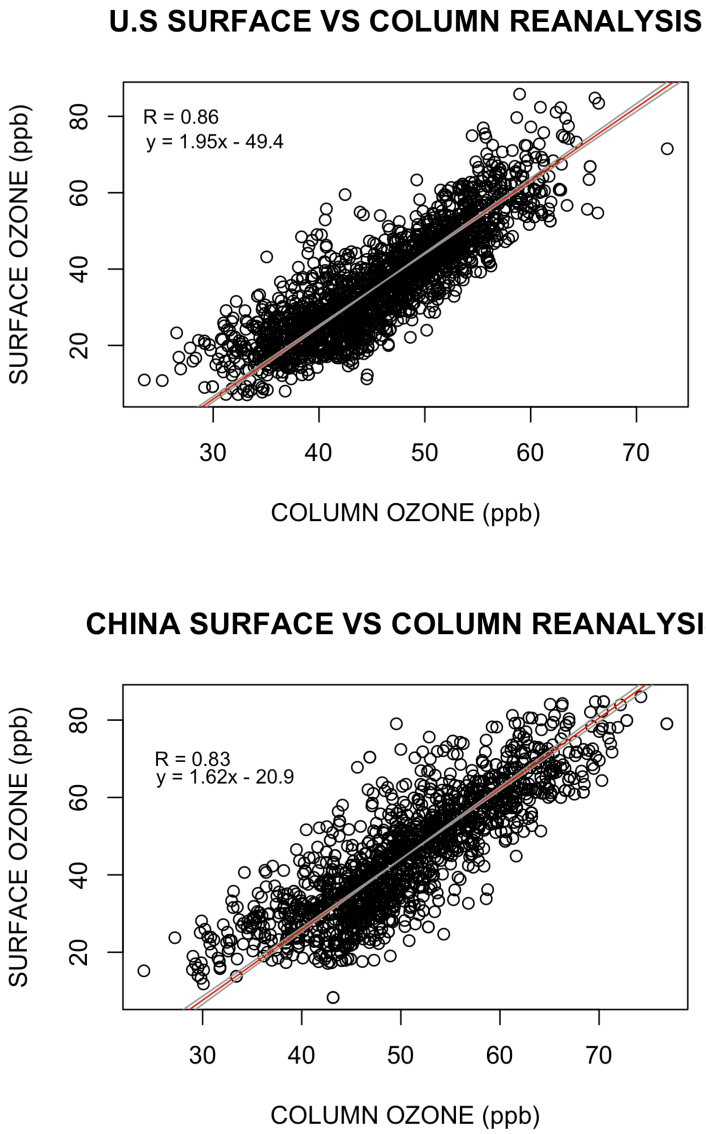

Figure 3. Scatter plots of summertime bias-corrected reanalysis surface (y-axis) and column (0-3 km) ozone at TES/OMI sampling sites (x-axis) for years 2005-2009 for (a) the United States and (b) China.

TES/OMI surface ozone for the eastern United States mainly reflects underestimation of ozone in the Northeast.

The SMA regression shows an R=0.69 and a slope of 1.4 for the United States, demonstrating that TES/OMI surface ozone inferences show a similar spatial pattern to temporally and spatially coincident TOAR grid points. Both data commonly reveal the highest surface ozone concentrations over the Southwestern United States and lowest concentrations over the Northeastern United States. A relatively large discrepancy (up to 5 ppb) between the surface ozone data is seen over the Southwestern United States,

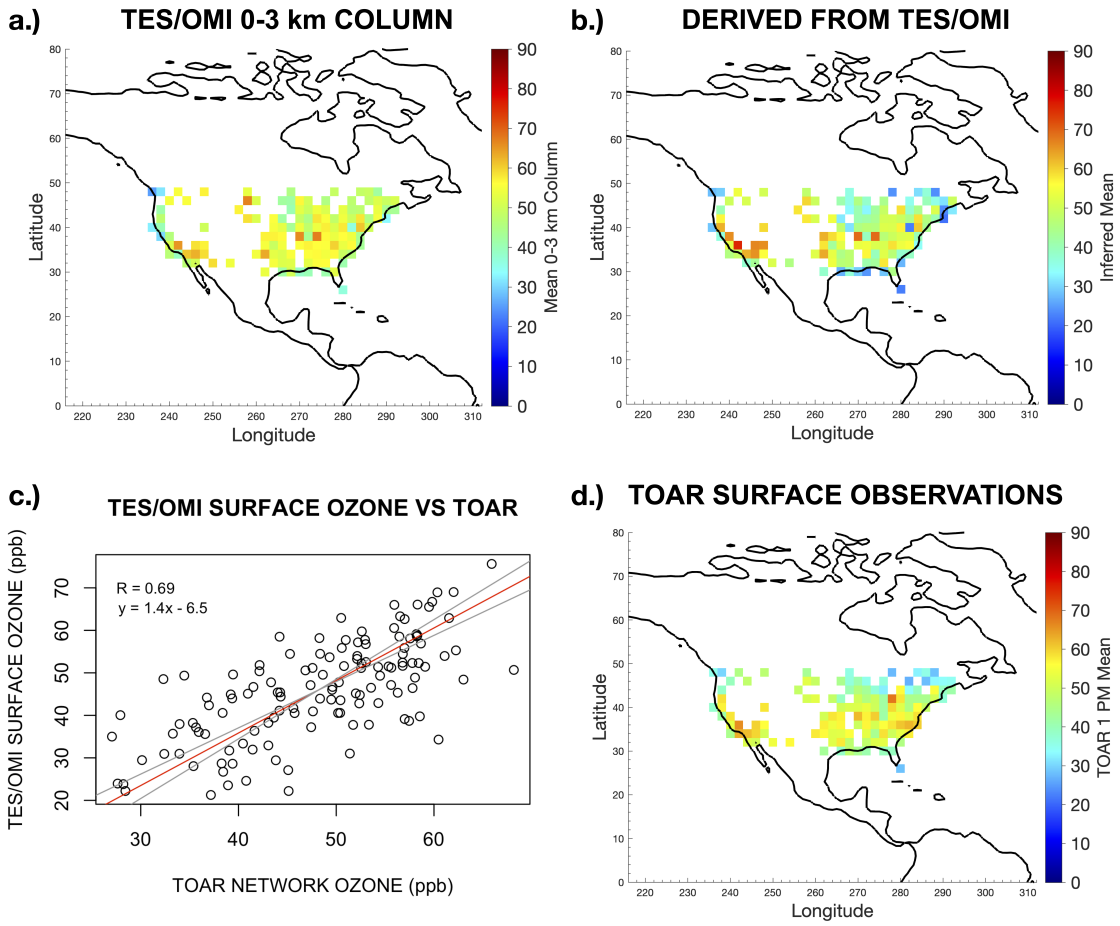

Figure 4. Spatial distributions of (a) TES/OMI mean 0-3 km column ozone concentrations averaged over JJA, (b) the TES/OMI inferred surface ozone (ppb), and (c) the surface ozone observations at 13:00 local time from the TOAR. (d) The scatter plots of the TES/OMI surface ozone inferences (y-axis) and the surface observations from the TOAR network (x-axis).

which could be affected by local bias in the surface to column relationship. At all sites, the surface ozone inferences show more variability than the TOAR observations, which could be attributed to random errors in TES/OMI data. While we focused on summer months, we find that the SMA regression for the United States for Fall (SON), Spring (MAM), and Winter (DJF) shows an R=0.64, R=0.54, and R=0.46 with slopes of 1.2, 1.4, and 1.5, respectively, in contrast to R=0.69 and a slope of 1.4 for Summer (JJA).

4.2.2. China For China (20N-50N, 100E-130E), the regional mean ozone concentration was 51.0 ppb for the TES/OMI 0-3 km column (Fig. 5a), 53.8 ppb (95% confidence interval [51.3 56.3] based on error in reanalysis bias) for the TES/OMI surface inferences (Fig. 5b), and 55.1 ppb for the MEE network (Fig. 5c), with increasing ozone from south to north across the country in all data. In Bejing, where high ozone is observed, mean

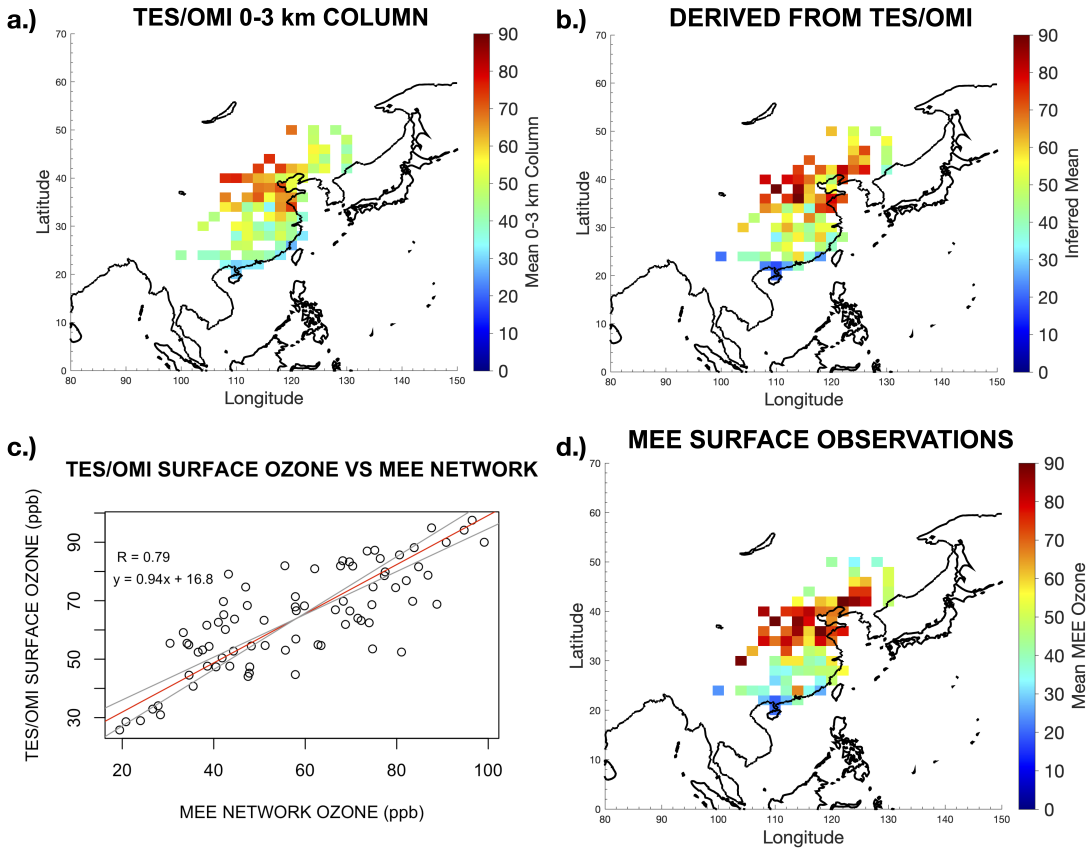

Figure 5. Same as in Fig. 4, but for China using the MEE surface observations.

JJA ozone in MEE was 72.1 ppb, similar to 69.0 ppb in the surface ozone inference. The surface ozone over Hong Kong shows anomalously high concentrations relative to the rest of Southern China, 54.7 ppb in MEE and 51.2 ppb in TES/OMI surface inferences. Overall, the TES/OMI surface ozone inferences capture the observed spatial ozone gradients. The overestimation by about 5 ppb in southern China is likely due to high levels of single scattering albedo (> 0.98) over these areas as seen in the OMI retrieval (Fig. S2), which may be indicative of confounding multiple scattering processes. The SMA regression shows an R=0.79 and a slope of 0.94 (Fig. 5d), demonstrating strong agreement between TES/OMI surface inferences and MEE network data.

We also compared TES/OMI inferences directly to MEE network data from the 2013-2017 period (Fig. S3 and S4). The converted MEE data for the 2005-2009 periods show better agreement with the satellite-derived surface ozone, demonstrating the power of the reanalysis for extending the spatial and temporal coverage of validation data.

We have taken the spatial standard deviation of the average summertime ozone concentrations from Figs. 4 and 5 in order to understand the differences in spatial variability of ozone for each dataset. The standard deviations (i.e spatial variability) are 7.5 ppb, 9.4 ppb, and 11.3 ppb for the TES/OMI 0-3 km column, TES/OMI surface

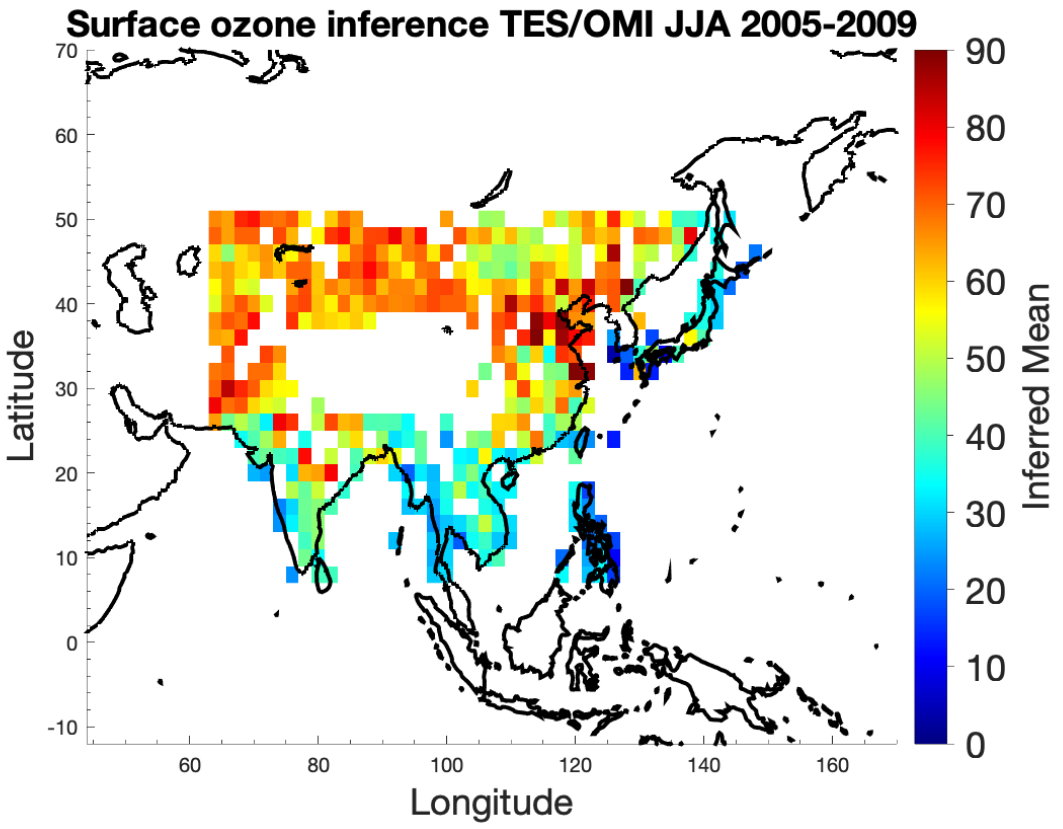

Figure 6. Estimated mean JJA surface ozone in Asia for 2005-2009.

inferences, and surface observations, respectively, for the United States, and 12.7 ppb, 13.7 ppb, and 15.6 ppb, respectively for China. For both regions, the TES/OMI 0-3 km column ozone shows less variability than the surface ozone inferences, in agreement with Fig. 3. Inferred surface ozone concentrations are lower over southern China and higher over northern China and the southwestern United States compared to the 0-3 km column. The fact that the variability in the TES/OMI surface inferences is higher than the ground networks for both regions may be due to random errors in TES/OMI data.

4.2.3. Broader Asia region We extended the analysis of ozone in China to a wider area in Asia (8-50N, 64-150E) that is largely unsampled in order to demonstrate the capability of the proposed approach to overcome the limitation of the current in-situ observing system (Fig. 6). The aforementioned bias corrections made for China are used for the entire East Asia region. This assumption may result in inaccurate bias corrections over some of the regions.

Although we cannot validate the surface ozone distribution because of the lack of independent observations, the general spatial structure is consistent with previous

studies and our understanding of ozone chemistry and transport. Overall, surface ozone patterns, such as high ozone in Northwestern China, are consistent between our TES/OMI inferences and a regional high-resolution chemical reanalysis [36] that assimilates surface measurements. The relatively low ozone concentrations over South Asia are consistent with the influence of the South Asian Monsoon, which leads to ozone-unfavorable meteorological conditions that suppresses chemical ozone production [37]. In northern India, hot spots in ozone generally correspond to enhanced NO_x emissions (Fig. S5) from coal fired power plants. The contrast between high ozone in North India and low ozone in South Asia in this season can be attributed to temporal differences in the start of the monsoon and the arrival of pristine marine air masses to the respective regions [38]. Summertime water vapor concentrations are significantly lower over North India compared to South Asia [38], which would also affect the regional differences in the relative balance of ozone production and loss. The high ozone in Mongolia and the Middle East correspond to a string of coal fired power plants (Fig. S5) surrounded by a low NO_x emitting region. Additionally, enhanced ozone in the Middle East during summer has been explained by the Arabian anticyclone, which facilitates large scale subsidence and the buildup of ozone [39],[40].

The high spatial variability in the ratio between reanalysis surface versus 0-3 km column ozone (Fig. S6) could reflect various factors, including near surface photochemical production, vertical mixing in the boundary layer, and convective transport. Strong photochemical production near the surface is expected to increase the ratio, whereas strong boundary layer mixing and convective transport act to flatten the vertical gradients. The overall spatial structure of the ratio can be largely affected by the presence of the Asian monsoon, which suppresses near surface photochemical ozone production, induces long-range transport of ozone-poor marine air masses into polluted areas in South and Southeast Asia [38]. These processes exhibit complex spatial and temporal patterns and inhibit understanding of surface ozone variations directly from the 0-3 km column.

In places with high NO_x emissions (Figure S5), such as northern China, a large surface:column ratio (nearly 2:1)implies high surface ozone and a boundary layer that is not well-mixed. In particular, persistent clear sky conditions in East Asia provide ozone-favorable meteorological conditions near the surface and inhibit vertical mixing. In contrast, there are various regions where we see a high ratio without high NO_x emissions, such as southern India and parts of the Middle East. This suggests that dynamics must play an important role, and could indicate that the 0-3 km column includes some free tropospheric air that is low in ozone concentration, which would act to increase the ratio. The estimated ratio from the reanalysis is close to 1:1 in Mongolia, suggesting that ozone within the boundary layer is well-mixed (Fig. S6).

5. Discussion

Exploring whether joint satellite retrievals have the capability to spatially resolve gradients in surface ozone is crucial in knowing the extent to which they can provide a tool to assess changes in air quality, especially in developing nations where few surface monitoring stations exist. Our results demonstrate the capability of combined UV and TIR instruments to detect spatial gradients in surface ozone when combined with a chemical reanalysis. This type of analysis can potentially be extended to provide global maps of surface ozone. The data could then be used to inform policy decisions and provide critical information relevant to human health in developing countries. However, the reanalysis used in this study does not provide urban scale surface to column relationship because of its relatively coarse spatial resolution. To explore urban scale changes, higher resolution reference data to convert satellite column to surface would be required.

Given the rapidly changing patterns of precursor emissions over the decade, including those of NO_x [41] and aerosols [42], it is likely that the relative contributions of local and non-local sources and consequent ozone variations are different between the TES/OMI analysis period (2005-2009) and more recent time periods. These temporal changes can be investigated by applying the approach proposed in this study to other satellite products such as AIRS+OMI, CrIS+OMPS, and IASI+GOME2 [16], [18] for the wider Asia region, along with surface measurements for limited areas.

The insights regarding the potential of combined UV+TIR retrievals to infer surface ozone gained in this paper come as a new wave of UV/VIS geostationary and Low Earth Orbiting (LEO) satellites aimed at observing air quality are launched. The Geostationary Environment Spectrometer (GEMS) ([43]), Sentinel-4, and Tropospheric Emissions: Monitoring of Pollution (TEMPO, [44]) missions will provide hourly measurements of tropospheric composition at high spatial resolution. Furthermore, recent UV/VIS LEO satellites including the Sentinel-5 Precursor [45], Sentinel-5 [46] and the Ozone Mapping and Profiler Suite (OMPS, [47]) provide daily measurements of global ozone profiles. While TIR composition measurements are available from meteorological sounders including AIRS, CrIS, IASI, and MetOP-SG, these instruments have coarser spectral resolution and thus lower tropospheric DOFS than TES. The combination of these instruments with UV/VIS instruments will provide less sensitivity to the 0-3 km ozone column than TES/OMI. Developing a satellite mission specifically aimed at combining TIR and UV/VIS radiances for optimizing the vertical sensitivity and resolution of ozone profiles near the surface is a crucial step forward in our ability to measure and understand changes in surface ozone in undersampled regions.

6. Conclusion

We have combined information from TES/OMI 0-3 km column retrievals and a chemical reanalysis in order to infer surface ozone concentrations for the United States, China, and broader Asia. The chemical reanalysis was used as a transfer function to convert the lower tropospheric column to surface ozone. Overall, the TES/OMI surface ozone inferences show a robust ability to capture the spatial gradient of ozone from south to north China, with a spatial correlation of 0.79. For the United States, they also show similar patterns to the TOAR observations, with a bias of < 1 ppb for the western U.S and < 4 ppb for the eastern U.S and a spatial correlation of R=0.69. The estimated surface ozone map for the broader Asia region can be explained by the Asian monsoon and the location of coal fired power plants and corresponding NO_x emissions. The obtained implications can further be explored in following studies, while expanding to other regions of the world.

Previous assessments of multispectral satellite instruments have focused on their ability to resolve ozone in the lower tropospheric column. The framework developed in this study provides a new way to determine detailed spatial gradients in surface ozone, by combining satellite retrievals with chemical reanalysis. This takes the analysis of multispectral instruments a step further and provides a better assessment of their ability to capture air quality variations. Furthermore, by converting column ozone measurements observed by the satellite observations to surface ozone inferences, we are able to better assess the sensitivity of the measurements by comparing them to surface network measurements as opposed to ozonesonde or aircraft data, the former of which provide a much higher volume of data in time and space.

Acknowledgements

We acknowledge the use of data products from the NASA AURA satellite missions. The TCR-2 dataset is available at: `https://doi.org/10.25966/9qgv-fe81`. The TES/OMI ozone level 2 data is available at: `https://doi.org/10.5067/AURA/TES-OMI/TOL2O3.003`. Part of this work was conducted at the Jet Propulsion Laboratory, California Institute of Technology, under contract with the National Aeronautics and Space Administration (NASA).

References

[1] Health Effects Institute. "State of Global Air 2019. Special Report". In: *JOURNAL OF GEOPHYSICAL RESEARCH: Atmospheres* (2019).

[2] ShiryAvnery. "Global crop yield reductions due to surface ozone exposure: 1. Year 2000 crop production losses and economic damage". In: *Atmospheric Environment* 45 (2011). DOI: https://doi.org/10.1016/j.atmosenv.2010.11.045.

[3] Gaudel et al. "Tropospheric Ozone Assessment Report: Present-day distribution and trends of tropospheric ozone relevant to climate and global atmospheric chemistry model evaluation". In: *Elem Sci Anth* 6 (2018). DOI: https://doi.org/10.1525/elementa.291.

[4] Kevin W. Bowman. "Toward the next Generation of Air Quality Monitoring: Ozone." In: *Atmospheric Environment* 80 (2013). DOI: https://doi.org/10.1016/j.atmosenv.2013.07.007.

[5] Guy P. Brasseur and Daniel J. Jacob. *Modeling of Atmospheric Chemistry*. Vol. 107. 1999. DOI: https://doi.org/10.1017/9781316544754.

[6] Randall V. Martin. "Satellite Remote Sensing of Surface Air Quality". In: *Atmospheric Environment* 42 (2008). DOI: https://doi.org/10.1016/j.atmosenv.2008.07.018.

[7] J. Landgraf and O.P Hasekamp. "The synergistic use of thermal infrared emission and ultraviolet reflectivity measurements from space". In: *J. Geophys. Res* 112 (2007). DOI: https://doi.org/10.1029/2006JD008097.

[8] X. Liu et al. "Ozone profile and tropospheric ozone retrievals from the Global Ozone Monitoring Experiment: Algorithm description and validation". In: *Journal of Geophysical Research: Atmospheres* 110 (2005). DOI: https://doi.org/10.1029/2005JD006240.

[9] X. Liu et al. "Ozone profile retrievals from the Ozone Monitoring Instrument". In: *Atmos. Chem. Phys* 10 (2010). DOI: https://doi.org/10.5194/acp-10-2521-2010.

[10] X. Liu et al. "First directly retrieved global distribution of tropospheric column ozone from GOME: Comparison to the GEOS-Chem model". In: *Journal of Geophysical Research: Atmospheres* 111 (2006). DOI: https://doi.org/10.1029/2005JD006564.

[11] C.D Rodgers. "Inverse methods for atmospheric sounding: Theory and practice". In: *Word Scientific Publishing, Singapore* (2000).

[12] John Worden et al. "Improved tropospheric ozone profile retrievals using OMI and TES radiances". In: *Geophysical Research Letters* 34 (2007). DOI: https://doi.org/10.1029/2006GL027806.

[13] D Fu et al. "Characterization of Ozone Profiles Derived from Aura TES and OMI Radiances." In: *Atmospheric Chemistry and Physics Discussions* 12 (2012). DOI: https://doi.org/10.5194/acpd-12-27589-2012.

[14] J. Cuesta et al. "Satellite observation of lowermost tropospheric ozone by multispectral synergism of IASI thermal infrared and GOME-2 ultraviolet measurements over Europe". In: *Atmos Chem Phys* 13 (2013). DOI: https://doi.org/10.5194/acp-13-9675-2013.

[15] Gaelle Dufour. "Lower tropospheric ozone over the North China Plain: variability and trends revealed by IASI satellite observations for 2008–2016". In: *Atmos. Chem. Phys* 18 (2018). DOI: https://doi.org/10.5194/acp-18-16439-2018.

[16] D. Fu. "Retrievals of tropospheric ozone profiles from the synergism of AIRS and OMI: Methodology and validation". In: *Atmospheric Measurement Techniques* 11 (2018). DOI: https://doi.org/10.5194/amt1155872018.

[17] VijayNatraj. "Multi-spectral sensitivity studies for the retrieval of tropospheric and lowermost tropospheric ozone from simulated clear-sky GEO-CAPE measurements". In: *Atmospheric Environment* 45 (2011). DOI: https://doi.org/10.1016/j.atmosenv.2011.09.014.

[18] Juan Cuesta et al. "Transboundary Ozone Pollution across East Asia: Daily Evolution and Photochemical Production Analysed by IASI + GOME2 Multispectral Satellite Observations and Models." In: *Atmospheric Chemistry and Physics* 18 (2018). DOI: https://doi.org/10.5194/acp-18-9499-2018.

[19] D Fu et al. "Characterization of Ozone Profiles Derived from Aura TES and OMI Radiances." In: *Atmospheric Chemistry and Physics Discussions* 12 (2013). DOI: https://doi.org/10.5194/acpd-12-27589-2012.

[20] Kazuyuki Miyazaki. "Updated tropospheric chemistry reanalysis and emission estimates, TCR-2, for 2005–2018". In: *Earth Syst. Sci. Data* 12 (2020). DOI: https://doi.org/10.5194/essd-12-2223-2020.

[21] Rienhard Beer. "TES on the Aura Mission: Scientific Objectives, Measurements, and Analysis Overview". In: *IEEE Trans. on Geosci. Remote Sensing* 44.5 (2006), pp. 1102–1105.

[22] Kevin W. Bowman et al. "Tropospheric Emission Spectrometer: Retrieval Method and Error Analysis". In: *IEEE Trans. on Geosci. Remote Sensing* 44 (2006). DOI: 10.1109/TGRS.2006.871234.

[23] D.B Jones. "Potential of observations from the Tropospheric Emission Spectrometer to constrain continental sources of carbon monoxide". In: *J. Geophys. Res.-Atmos* 108 (2003). DOI: https://doi.org/10.1029/2003JD003702,2003.

[24] K. Miyazaki, H. J. Eskes, and K. Sudo. "A Tropospheric Chemistry Reanalysis for the Years 2005–2012 Based on an Assimilation of OMI, MLS, TES, and MOPITT Satellite Data". In: *Atmospheric Chemistry and Physics* 15 (2015). DOI: https://doi.org/10.5194/acp-15-8315-2015.

[25] Martin G. Schultz et al. "Tropospheric Ozone Assessment Report: Database and Metrics Data of Global Surface Ozone Observations". In: *Elem Sci Anth* 5 (2017). DOI: https://doi.org/10.1525/elementa.244.

[26] Kazuyuki Miyazaki. "Balance of Emission and Dynamical Controls on Ozone During the Korea-United States Air Quality Campaign From Multiconstituent Satellite Data Assimilation". In: *Journal of Geophysical Research: Atmospheres* 124 (2018). DOI: https://doi.org/10.1029/2018JD028912.

[27] Kazuyuki Miyazaki et al. "Evaluation of a multi-model, multi-constituent assimilation framework for tropospheric chemical reanalysis". In: *Atmos. Chem. Phys.* 20 (2020). DOI: https://doi.org/10.5194/acp-20-931-2020.

[28] Kazuyuki Miyazaki. "Air quality response in China linked to the 2019 novel Coronavirus (COVID-19) mitigation". In: *Geophysical research letters* 47 (2020). DOI: https://doi.org/10.1029/2020GL089252.

[29] K. Miyazaki et al. "Global tropospheric ozone responses to reduced NOx emissions linked to the COVID-19 world-wide lockdowns". In: *Science Advances* (2021). DOI: inpress.

[30] Le Kuai. "Attribution of Chemistry-Climate Model Initiative (CCMI) ozone radiative flux bias from satellites". In: *Atmos. Chem. Phys* 20 (2020). DOI: https://doi.org/10.5194/acp-20-281-2020.

[31] Benjamin Gaubert. "Correcting model biases of CO in East Asia: impact on oxidant distributions during KORUS-AQ". In: *Atmospheric Chemistry and Physics* 20 (2020). DOI: https://doi.org/10.5194/acp-20-14617-2020.

[32] Kazuyuki Miyazaki. "Global tropospheric ozone responses to reduced NOx emissions linked to the COVID-19 worldwide lockdowns". In: *Science Advances* 7 (2021). DOI: https://doi.org/10.1126/sciadv.abf7460.

[33] Herman G. J. Smit. "Assessment of the performance of ECC-ozonesondes under quasi-flight conditions in the environmental simulation chamber: Insights from the Juelich Ozone Sonde Intercomparison Experiment (JOSIE)". In: *Journal of Geophysical Research: Atmospheres* 112 (2007). DOI: https://doi.10.1029/2006JD007308.

[34] Katherine Travis. "Why do models overestimate surface ozone in the Southeast United States?" In: *Atmos. Chem. Phys* 16 (2016). DOI: https://doi.org/10.5194/acp-16-13561-2016.

[35] Kazuyuki Miyazaki and Kevin Bowman. "Evaluation of ACCMIP ozone simulations and ozonesonde sampling biases using a satellite-based multi-constituent chemical reanalysis". In: *Atmos. Chem. Phys* 17 (2017). DOI: https://doi.org/10.5194/acp-17-8285-2017.

[36] Lei Kong. "A 6-year-long (2013–2018) high-resolution air quality reanalysis dataset in China based on the assimilation of surface observations from CNEMC". In: *Earth System Science Data* 13 (2021). DOI: https://doi.org/10.5194/essd-13-529-2021.

[37] Xiao Lu. "Lower tropospheric ozone over India and its linkage to the South Asian monsoon". In: *Atmos. Chem. Phys* 18 (2018). DOI: https://doi.org/10.5194/acp-18-3101-2018.

[38] R. Kumar. "Simulations over South Asia using the Weather Research and Forecasting model with Chemistry (WRF-Chem): chemistry evaluation and initial results". In: *Geosci. Model Dev* 5 (2012). DOI: https://doi.org/10.5194/gmd-5-619-2012.

[39] Qinbin Li. "A tropospheric ozone maximum over the Middle East". In: *Geophysical Research Letters* 28 (2001). DOI: https://doi.org/10.1029/2001GL013134.

[40] Jane J. Liu. "Analysis of the summertime buildup of tropospheric ozone abundances over the Middle East and North Africa as observed by the Tropospheric Emission Spectrometer instrument". In: *Geophysical Research Letters* 114 (2009). DOI: https://doi.org/10.1029/2008JD010993.

[41] Kazuyuki Miyazaki. "Decadal changes in global surface NOx emissions from multi-constituent satellite data assimilation". In: *Atmos. Chem. Phys* 17 (2017). DOI: https://doi.org/10.5194/acp-17-807-2017.

[42] Jia Xing. "Impacts of aerosol direct effects on tropospheric ozone through changes in atmospheric dynamics and photolysis rates". In: *Atmos. Chem. Phys* 17 (2017). DOI: https://doi.org/10.5194/acp-17-9869-2017.

[43] Jhoon Kim et al. "New Era of Air Quality Monitoring from Space: Geostationary Environment Monitoring Spectrometer (GEMS)". In: *Bulletin of the American Meteorological Society Bulletin of the American Meteorological Society* 101 (2020). DOI: https://doi.org/10.1175/BAMS-D-18-0013.1.

[44] P. Zoogman et al. "Tropospheric emissions: Monitoring of pollution (TEMPO)". In: *J. Quant. Spectrosc. Ra* 186 (2017). DOI: https://doi.org/10.1016/j.jqsrt.2016.05.008.

[45] Veefkind et al. "TROPOMI on the ESA Sentinel-5 Precursor: A GMES mission for global observations of the atmospheric composition for climate, air quality and ozone layer applications". In: *Remote Sensing of the Environment* 120 (2012). DOI: https://doi.org/10.1016/j.rse.2011.09.027.

[46] P. Ingman et al. “Requirements for the GMES Atmosphere Service and ESA’s implementation concept: Sentinels-4/-5 and -5p”. In: *Remote Sensing of the Environment* 120 (2012). DOI: https://doi.org/10.1016/j.rse.2012.01.023.

[47] L.E Flynn et al. “The Ozone Mapping and Profiler Suite.” In: *Earth Science Satellite Remote Sensing* (2006). DOI: https://doi.org/10.1007/978-3-540-37293-6_15.